Kapal: Jurnal Ilmu Pengetahuan dan Teknologi Kelautan
(Kapal: Journal of Marine Science and Technology)
journal homepage : http://ejournal.undip.ac.id/index.php/kapal
2301-9069 (e)
1829-8370 (p)

Structural Design Analysis of Sandwich Cylindrical Shells Under Axial Compression Load: Utilization of Geometry and Material Variations

Muhammad Daffa Alifianto[1)], Hamdani Maftuh Rohman[1)], Anandito Adam Pratama[1)], Iwan Istanto[1)], Aditya Rio Prabowo[1)*)], Oleksiy Melnyk[2)], Quang Thang Do[3)], Teguh Muttaqie[4)], Eko Prasetya Budiana[1)], Jung Min Sohn[5,6)], Rahman Wijaya[1)]

[1)] Department of Mechanical Engineering, Universitas Sebelas Maret, Surakarta, Indonesia
[2)] Department of Navigation and Maritime Safety, Odesa National Maritime University, Odesa, Ukraine
[3)] Department of Naval Architecture and Ocean Engineering, Nha Trang University, Nha Trang, Viet Nam
[4)] Research Center for Hydrodynamics Technology, National Research and Innovation Agency (BRIN), Surabaya, Indonesia
[5)] Department of Naval Architecture and Marine Systems Engineering, Pukyong National University, Busan, South Korea
[6)] Department of Marine Design Convergence Engineering, Pukyong National University, Busan, South Korea
[*)] Corresponding Author: aditya@ft.uns.ac.id

Article Info

Keywords:
Sandwich Cylindrical Shell;
Finite Element Method;
Von Mises Stress;
Displacement;
Energy Absorption.

Article history:
Received: 14/07/2025
Last revised: 11/09/2025
Accepted: 14/09/2025
Available online: 15/09/2025
Published: 31/10/2025

DOI:
https://doi.org/10.14710/kapal.v22i3.75955

Abstract

This study aims to analyze the performance of sandwich cylindrical shell structures under axial compression load by varying the geometry and types of material. Numerical simulations were conducted using ABAQUS software, employing the finite element method (FEM) to evaluate von Mises stress, displacement, and energy absorption. The materials used include ASTM 1045, ASTM A36, and Mild Steel, with geometry designs varying across five different configurations. The simulation results indicate that the combination of material and geometry has a significant impact on the structural response of the sandwich cylindrical shell. ASTM 1045 exhibited the highest von Mises stress and displacement, indicating both high strength and substantial deformation, while Mild Steel demonstrated better elastic properties. Geometry 4 combined with ASTM 1045 proved to be the strongest configuration, while the combination of Geometry 1 and Mild Steel was the most elastic. This study contributes to the development of more efficient and impact-resistant ship structural designs.

1. Introduction

Indonesia is the largest archipelagic country in the world, boasting a lengthy coastline and extensive waters. This makes the maritime sector one of the backbones of the national economy, with the shipbuilding industry playing a vital role in transportation, fisheries, and naval defence. As the world's largest archipelago, Indonesia possesses extraordinary marine wealth. With more than 17,000 islands and a coastline stretching 95,161 kilometres [1]. This unique geographical condition makes the maritime sector a backbone of the national economy, where the shipbuilding industry plays a vital role in transportation, fisheries, and naval defence. Indonesia's abundant marine wealth and the strategic function of its seas as major transportation routes domestically and internationally demand innovation and technological advancement, especially in the shipbuilding sector [2].

One of the key innovations in this industry is the use of sandwich cylindrical shell structures, which are composite structures consisting of two strong and lightweight outer skins enclosing a thicker yet lighter core [3,4]. This structure offers a combination of high strength and low weight, making it ideal for ship construction [5]. In the harsh maritime environment, ships must resist corrosion, possess structural strength, and maintain fuel efficiency. A sandwich shell enhances ship performance in terms of speed, stability, and durability while reducing operational costs [6]. Adopting sandwich shell technology can improve the global competitiveness of Indonesia's shipbuilding industry. Ships made with sandwich shells offer advantages in energy efficiency and lower maintenance costs, which are critical for long-term operations [7,8]. Furthermore, this technology contributes to reducing carbon emissions, aligning with global efforts to mitigate climate change [9,10]. Therefore, integrating sandwich shell structures in ship construction is a strategic step in line with Indonesia's vision to become a global maritime axis.

To support this advancement, the study aims to analyse the structural response of sandwich shells under axial compression, focusing on various geometric configurations and material combinations. Furthermore, the research aims to identify both the best- and worst-case performance scenarios, providing valuable insights into the optimal material selection and design strategies for maritime applications.

2. Method

2.1. Benchmarking procedures

Vehicle collisions generally occur in two primary forms: axial impacts and angular impacts [11],[12]. Numerous studies have explored ways to enhance vehicle crash resistance, such as the use of front spring dampers. Although this topic has produced significant findings, few previous studies have focused on the effects of gradient layers. In this study, the researchers proposed a new cylindrical rod, examined comprehensively with an emphasis on the gradient layer. It is assumed that the plate used as the base of the tube is rigid. Subsequently, the cylindrical tube is subjected to a rigid impactor moving axially at an initial speed of 12.5 m/s with a mass of 200 kg.

Several studies have been conducted on structural analysis under compression conditions. Pratama et al. [13] investigated axial dynamic crushing of square and circular tubes. The same author later studied typical failure modes of square pipes. Over time, thin-walled structures have become widely used in transportation systems as energy absorbers during crashes and other accidents [14]. Tak and Iqbal [15] studied thin-walled structures in the form of hollow tubes as energy absorbers subjected to various compressive loads. Thin-walled structures help minimize damage from collisions, including with ships, in the form of crash boxes, as used in automobiles [16].

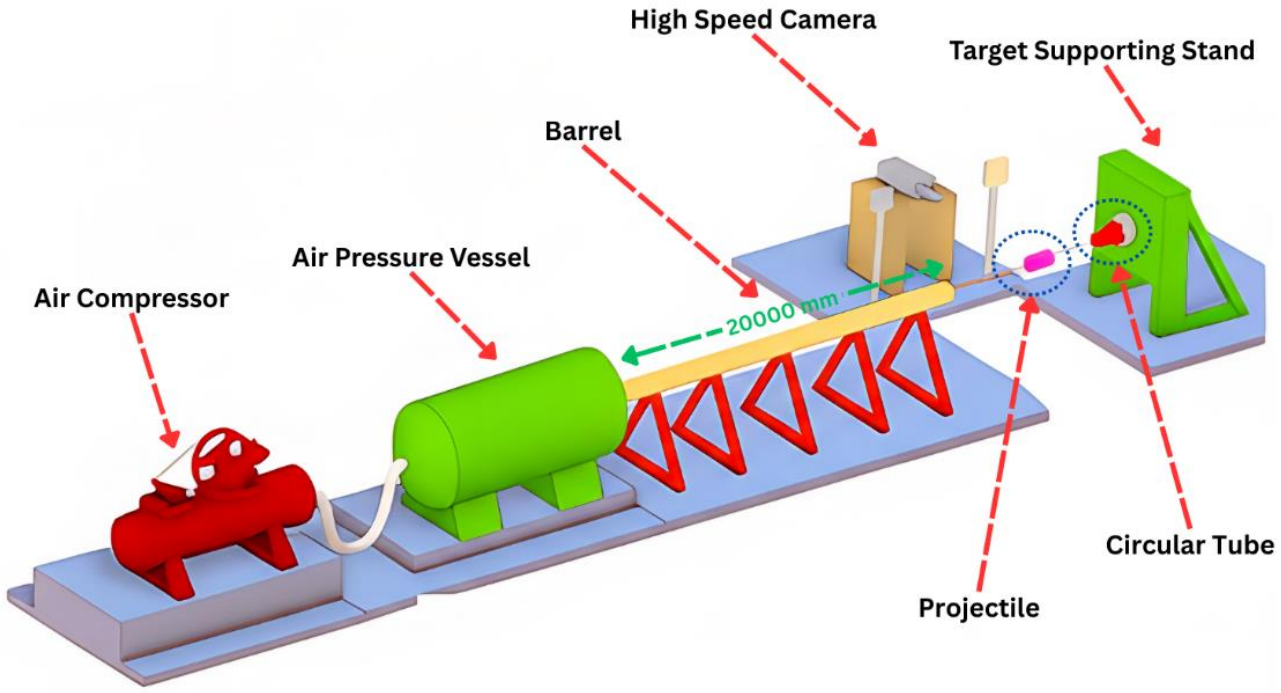

Figure 1. Axial Compression Testing Procedure (redrawn based on [15])

Figure 1 illustrates the experimental system for dynamic axial compression testing using an air-based launcher. This system is used to fire a projectile at a target tube (a circular tube) to investigate the deformation behaviour and energy absorption of the tube under high-speed axial compression. For this test, a hollow tube design and a 2D-designed projectile are used, as shown in Figure 2.

Figure 3 shows the geometric simulation model used for benchmarking purposes, which consists of two main components: the impactor and the hollow. The impactor is a solid object that strikes the hollow cylindrical tube, generating an axial compression load. Meanwhile, the hollow is the primary test object–a hollow cylindrical tube simulated to receive force from the impactor. The simulation can be considered successful if the results deviate by no more than 10% from the benchmarking reference, as shown in Figure 4, which presents the benchmarking results.

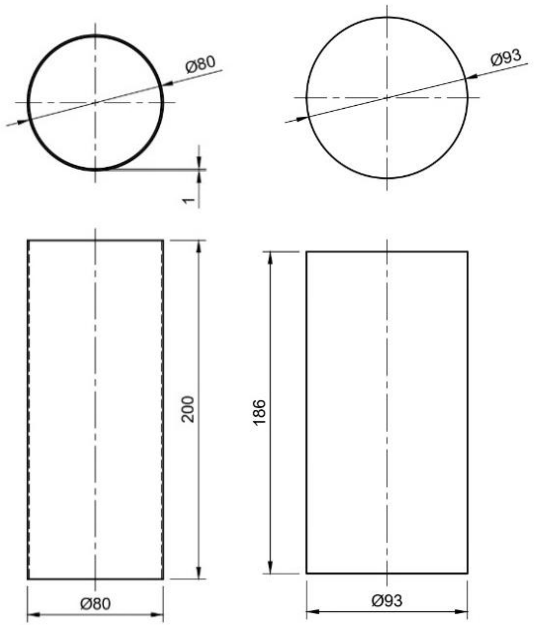

Figure 2. 2D Benchmarking of Hollow Tube Design

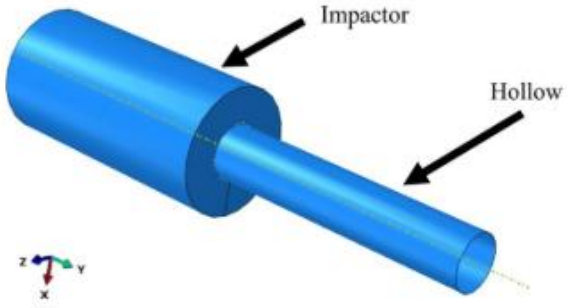

Figure 3. Benchmarking Model Geometry

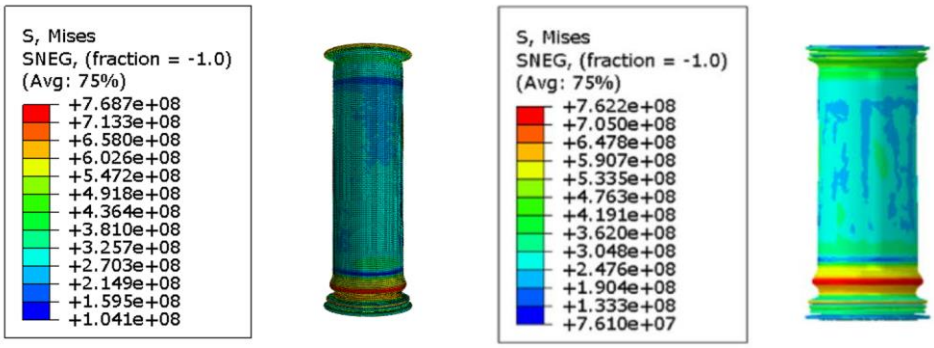

Figure 4. Benchmarking of Von-Mises Contour

2.2. Geometrical Models

In this study, the geometry used for simulating impact conditions is a sandwich cylindrical shell structure on a tanker ship. This structure is modelled using ABAQUS software with a shell model having a thickness of 1 mm and consists of five different geometric variations. Overall, the sandwich shell structure has an outer diameter of 80 mm, an inner diameter of 60 mm, and a height of 200 mm. This structure will be compressed using an impactor with a diameter of 93 mm and a height of 186 mm, as shown in Figure 5 and the technical drawing in Figure 6.

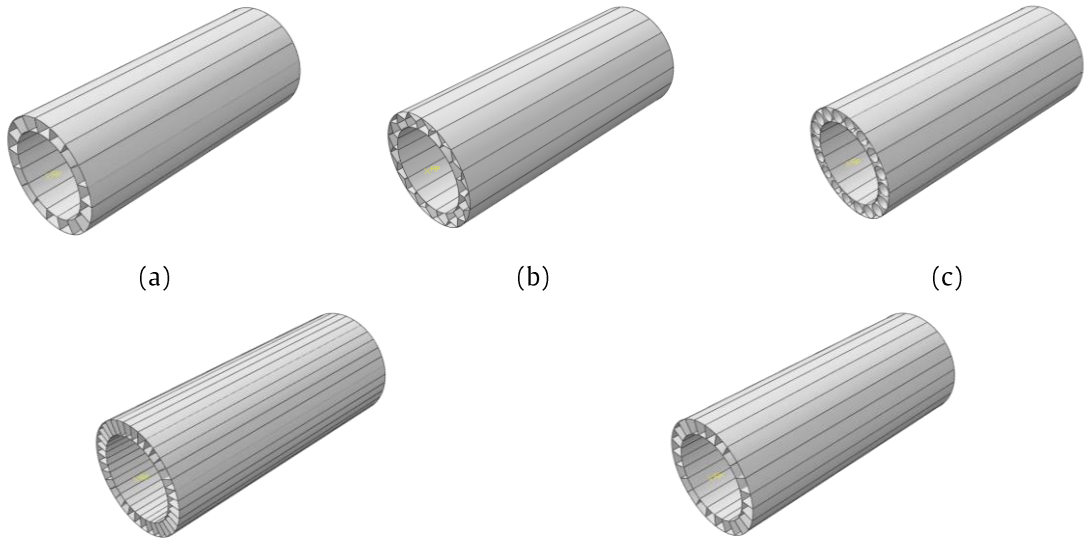

(a) (b) (c) (d) (e)

Figure 5. Sandwich Cylindrical Shell 3D Models: (a) Geometry 1, (b) Geometry 2, (c) Geometry 3, (d) Geometry 4, and (e) Geometry 5

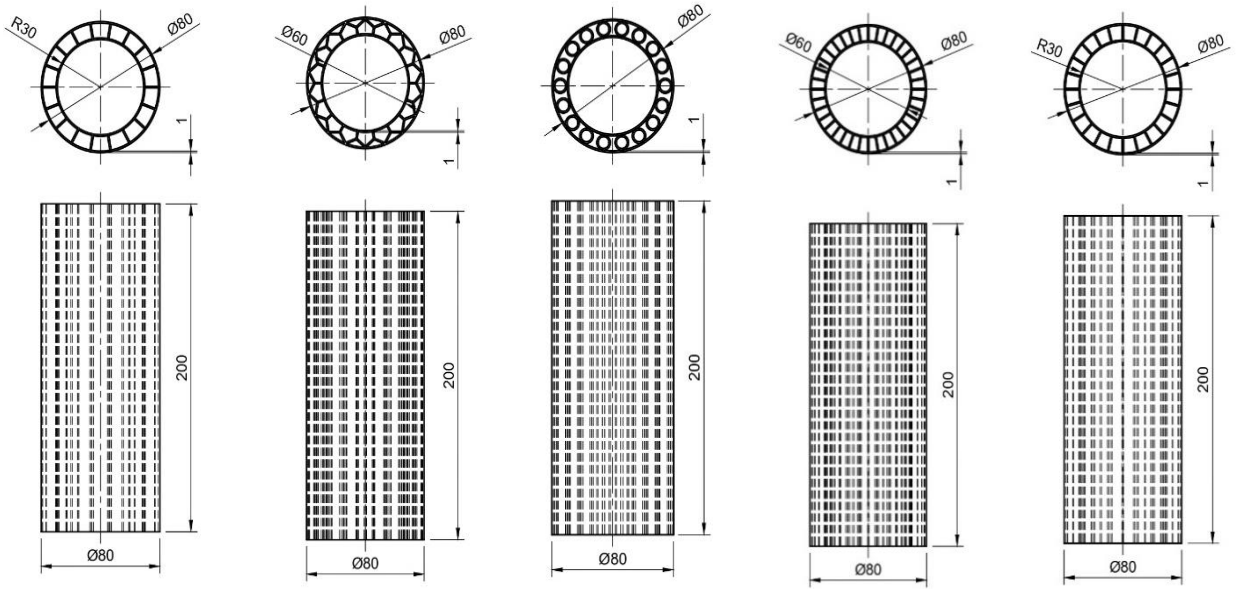

(a) (b) (c) (d) (e)

Figure 6. 2D Designs of Sandwich Shells: (a) Geometry 1, (b) Geometry 2, (c) Geometry 3, (d) Geometry 4, and (e) Geometry 5

2.3. Johnson-Cook Failure Model

As stated in previous studies [15], the Johnson-Cook isotropic constitutive hardening and failure model [17], can be used to characterize the material model applied in the simulation. This model incorporates material flow based on linear thermo-elasticity, the von Mises yield criterion, isotropic strain hardening, strain rate hardening, and thermal softening due to adiabatic effects. The equivalent von Mises stress σ in the Johnson-Cook model is expressed as:

$$\bar{\sigma}\left(\bar{\varepsilon}^{pl}, \dot{\bar{\varepsilon}}^{pl}, \hat{T}\right) = \left[A + B(\bar{\varepsilon}^{pl})^{n}\right]\left[1 + C ln\left(\frac{\dot{\bar{\varepsilon}}^{pl}}{\dot{\bar{\varepsilon}}_0}\right)\right]\left[1 - \hat{T}^{m}\right] \quad (1)$$

where, A, B, n, C, and m are material parameters obtained from various experiments. $\dot{\bar{\varepsilon}}_0$ is the reference strain rate, $\bar{\varepsilon}^{pl}$ is the equivalent plastic strain, and $\hat{T}$ is a unitless temperature-related parameter defined as:

$$\hat{T} = \frac{T - T_0}{T_{melt} - T_0} \quad (2)$$

The Johnson-Cook fracture model requires the strain rate, the effect of stress triaxiality, and temperature on the equivalent failure strain. The equivalent fracture strain in the Johnson-Cook model is expressed as:

$$\bar{\varepsilon}_f^{pl}\left(\frac{\sigma_m}{\bar{\sigma}}, \dot{\bar{\varepsilon}}^{pl}, \hat{T}\right) = \left[D_1 + D_2\, exp\left(D_3 \frac{\sigma_m}{\bar{\sigma}}\right)\right]\left[1 + D_4\, ln\left(\frac{\dot{\bar{\varepsilon}}^{pl}}{\dot{\varepsilon}_0}\right)\right][1 + D_5\, \hat{T}] \quad (3)$$

where D_1 to D_5 are material parameters determined from various mechanical tests. D_1, D_2, and D_3 are stress triaxiality parameters, D_4 is a damage parameter dependent on strain rate, and D_5 is a fracture strain parameter dependent on temperature., $\frac{\sigma_m}{\bar{\sigma}}$ is the stress triaxiality ratio, where σ_m is the mean stress and $\bar{\sigma}$ is the equivalent von Mises stress.

2.4. Material Definition

The materials used in this study comprise three types commonly employed in ship structures. These materials are ASTM A36, ASTM 1045, and mild steel. In the ABAQUS software, to perform impact simulations using the axial compression method, it is necessary to input not only general material properties such as yield strength, Young's modulus, and density, but also Johnson-Cook damage parameters, as shown in Table 1 [18].

Table 1. Applied Material Properties of Sandwich Shells.

Parameter	Mild Steel	ASTM A36	ASTM 1045
Density, ρ (kg/m³)	7850	7850	7810
Modulus of elasticity, E (N/m²)	203× 10^9	200 × 10^9	205 × 10^9
Poisson's ratio, v	0.33	0.26	0.29
Johnson–Cook flow stress parameters:			
Initial yield stress, A (N/m²)	304.33 × 10^6	250 × 10^6	506 × 10^6
Hardening coefficient, B (N/m²)	422 × 10^6	477 × 10^6	320 × 10^6
Hardening exponent, n	0.345	0.18	0.28
Strain rate constant, C	0.0156	0.012	0.064
Thermal softening constant, m	0.87	1	1.06
Reference strain rate, $\dot{\varepsilon}_0$(s−1)	0.0001	0.0001	0.0001
Melting temperature, T_{melt}(K)	1800	1811	1733
Transition temperature, T_0(K)	293	300	300
Johnson–Cook Fracture strain constant:			
D1	304.33 × 10^6	250 × 10^6	506 × 10^6
D2	422 × 10^6	477 × 10^6	320 × 10^6
D3	0.345	0.18	0.28
D4	0.0156	0.012	0.064
D5	0.87	1	1.06

2.5. Meshing Strategy

In numerical simulation methods, meshing is one of the most critical components that can affect the accuracy of the simulation results [19]. Therefore, selecting the appropriate element type and mesh size is essential to improve the accuracy of simulations performed using the finite element method. In this study, a mesh size of 0.009 m was used with the S4R Shell Element type. This element type and size were chosen because they had reached stability for conducting the compression simulation [20]. An illustration of the mesh used in this simulation is shown in Figure 7.

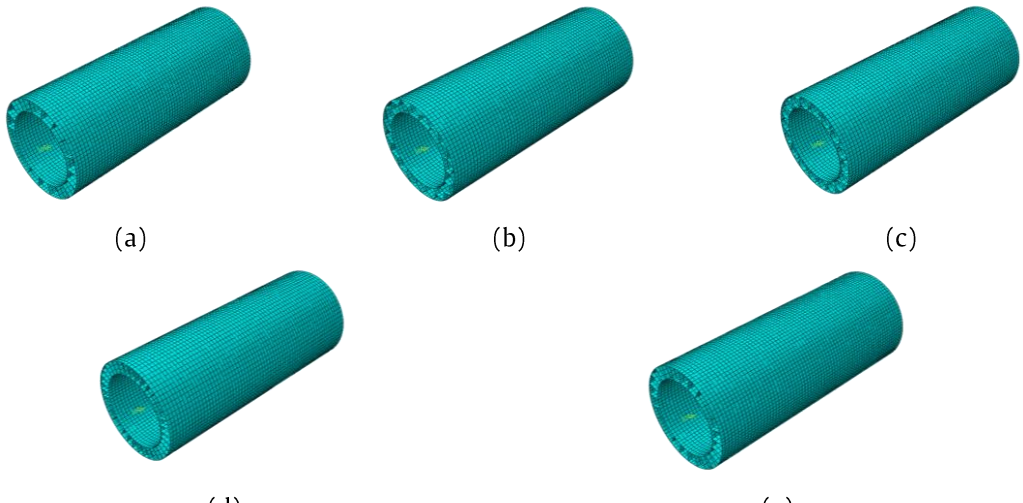

(a) (b) (c) (d) (e)

Figure 7. Mesh Configurations: (a) Geometry 1, (b) Geometry 2, (c) Geometry 3, (d) Geometry 4, and (e) Geometry 5

2.6. Boundary Condition

To represent a simulation that closely resembles realistic conditions, boundary conditions are applied to both sides of the structure, with displacement constraints on one side and encased (fixed) conditions on the opposite side. Figure 8 illustrates how the boundary conditions are applied to the sandwich shell structure. In axial compression, displacement-type boundary conditions are applied to the upper part of the shell to determine the maximum displacement imposed on the structure. Additionally, axial compression is used by assigning a velocity to the impactor, which compresses the sandwich shell until the maximum pressure is reached. The simulation is conducted over a time of 0.2 seconds, with geometric variations to observe differences in structural damage for each geometry.

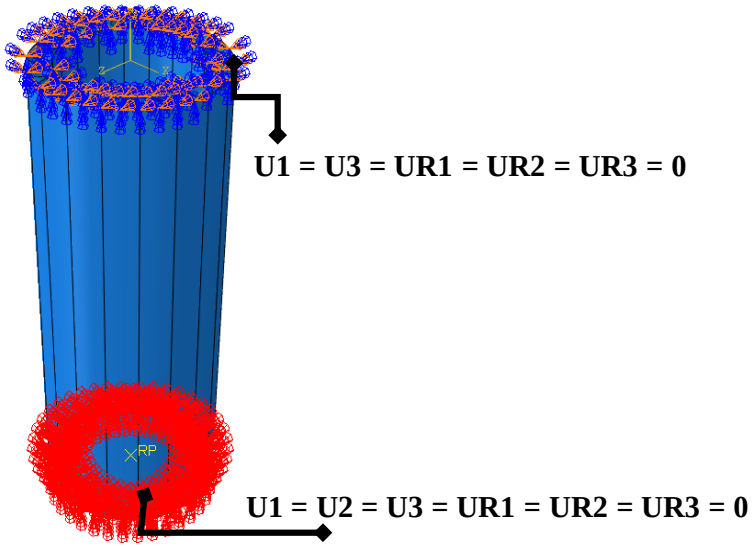

Figure 8. Boundary Conditions

2.7. Scenario Case

In this study, several scenarios were designed to simulate axial compression based on variations in parameters, namely geometry and material type used in the model. This study aims to investigate the outcomes resulting from the differences in these two parameters in more detail. The scenarios applied to the model are presented in Table 2.

Table 2. Summary of the simulation Scenarios.

Notation	Geometry	Material	Velocity (m/s)	Time (s)
Model 1	Geometry 1	Mild Steel	12.5	0.2
Model 2	Geometry 2	Mild Steel	12.5	0.2
Model 3	Geometry 3	Mild Steel	12.5	0.2
Model 4	Geometry 4	Mild Steel	12.5	0.2
Model 5	Geometry 5	Mild Steel	12.5	0.2
Model 6	Geometry 1	ASTM A36	12.5	0.2
Model 7	Geometry 2	ASTM A36	12.5	0.2
Model 8	Geometry 3	ASTM A36	12.5	0.2
Model 9	Geometry 4	ASTM A36	12.5	0.2
Model 10	Geometry 5	ASTM A36	12.5	0.2
Model 11	Geometry 1	ASTM 1045	12.5	0.2
Model 12	Geometry 2	ASTM 1045	12.5	0.2
Model 13	Geometry 3	ASTM 1045	12.5	0.2
Model 14	Geometry 4	ASTM 1045	12.5	0.2
Model 15	Geometry 5	ASTM 1045	12.5	0.2

3. Results and Discussion

3.1. Effect of Material Type

In the simulations conducted, material differences were one of the key factors contributing to variations in the results under axial compression conditions. This is due to the differing properties of each material used. To determine these differences, simulations were conducted by applying a pressure at a velocity of 12.5 m/s over 0.2 seconds. The results show overall differences in the von Mises stress contours, as illustrated in Figure 9 to 13.

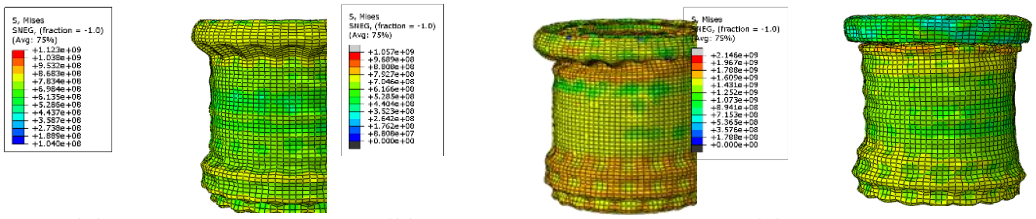

(a) (b) (c)

Figure 9. Von Mises Stress Contour on Geometry 1 with Material Variations: (a) Mild Steel, (b) ASTM A36, and (c) ASTM 1045

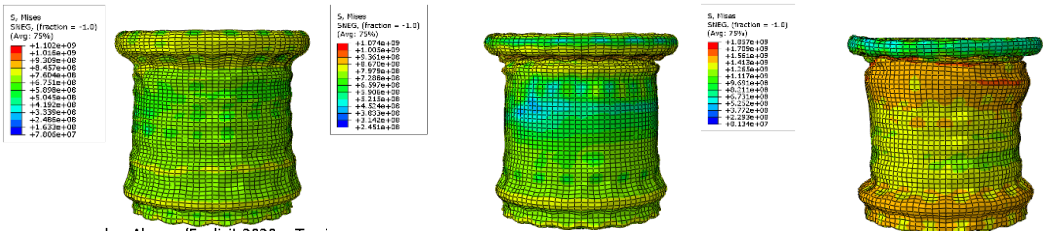

(a) (b) (c)

Figure 10. Von Mises Stress Contour on Geometry 2 with Material Variations: (a) Mild Steel, (b) ASTM A36, and (c) ASTM 1045

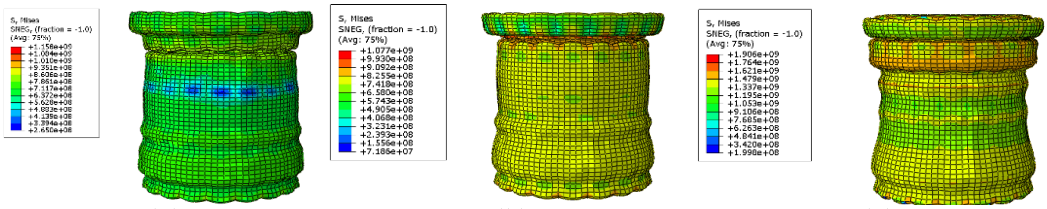

(a) (b) (c)

Figure 11. Von Mises Stress Contour on Geometry 3 with Material Variations: (a) Mild Steel, (b) ASTM A36, and (c) ASTM 1045

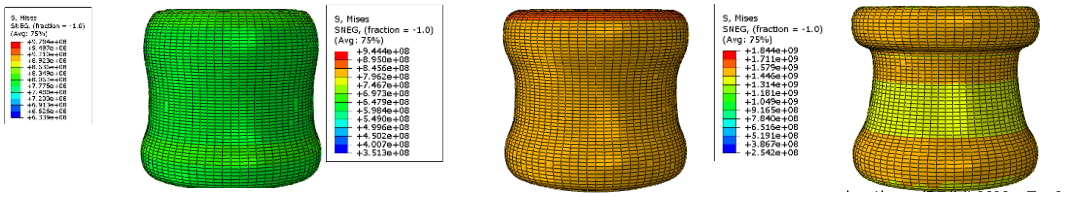

(a) (b) (c)

Figure 12. Von Mises Stress Contour on Geometry 4 with Material Variations: (a) Mild Steel, (b) ASTM A36, and (c) ASTM 1045

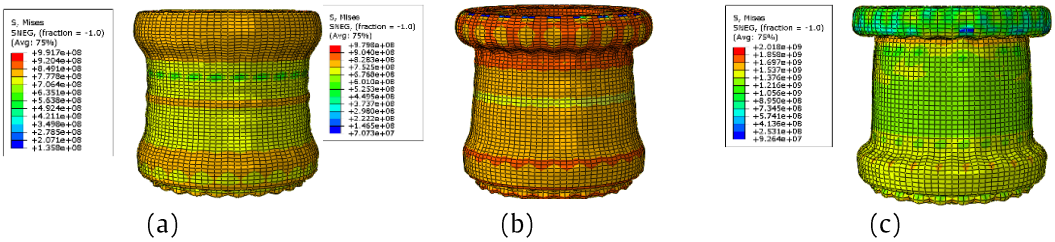

(a) (b) (c)

Figure 13. Von Mises Stress Contour on Geometry 5 with Material Variations: (a) Mild Steel, (b) ASTM A36, and (c) ASTM 1045

Based on Figure 9 to 13, the three tested materials exhibit distinct mechanical behaviours and failure modes influenced by the structural geometry used. ASTM A36, with the lowest yield strength of 250 MPa but the highest strain hardening coefficient at 477 MPa, demonstrates excellent energy absorption through stable and progressive deformation. In the longitudinal stiffener configuration (geometries 1, 4, and 5), ASTM A36 displays flexible and consistent local buckling patterns across the cylindrical shells. For the diagonal grid stiffener (geometry 2), the diamond-shaped shells undergo significant stretching and bulging, enabling uniform energy distribution throughout the structure. Meanwhile, in the ring stiffener configuration (geometry 3), the material forms tight and uniform concertina folds, indicating highly efficient energy absorption through controlled deformation.

Mild Steel balances strength and ductility effectively. With an initial yield strength of 304.33 MPa and a strain hardening coefficient of 422 MPa, it presents an optimal compromise, sustaining higher initial loads without sacrificing the stable deformation behavior observed in ASTM A36. The failure mode in the longitudinal stiffener arrangement resembles that of ASTM A36 but requires greater load levels to initiate. In diagonal grid and ring stiffener configurations, Mild Steel maintains

ideal stiffness combined with effective plastic deformation, producing concertina folds that tend to be larger and fewer compared to ASTM A36, thereby enhancing overall structural stability.

ASTM 1045 outperforms the other materials in terms of strength and stiffness. With a high yield strength of 506 MPa but a comparatively lower strain hardening coefficient of 320 MPa, it withstands the highest load capacities across all configurations. However, its deformation becomes more concentrated and less uniform. In the ring stiffener setup, concertina folds are fewer but larger, indicating that each fold absorbs substantial energy. The advantages of ASTM 1045 are most pronounced in stiff and robust structures, such as the diagonal grid and longitudinal stiffeners, where the synergy of material strength and geometric stiffness yields highly resilient tubes, albeit at the cost of reduced energy dissipation efficiency.

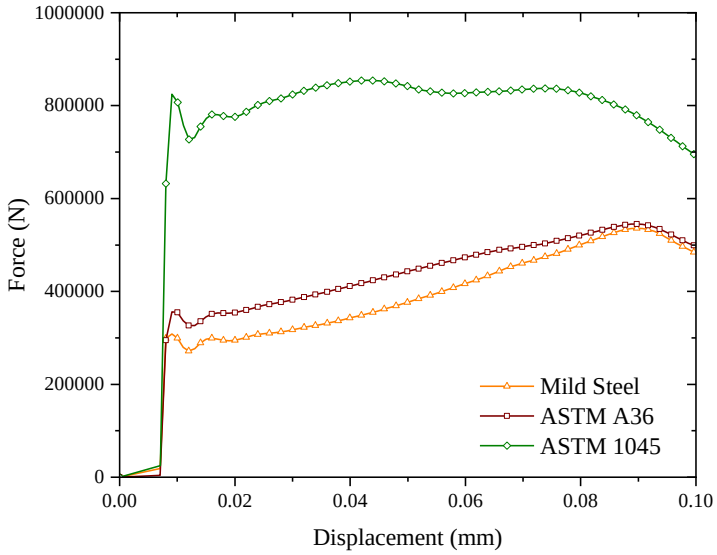

Figure 14. Displacement Graph of Material Variations

Examining displacement trends in Figure 14 reveals that ASTM 1045 experiences minimal displacement, correlating with its high stiffness and concentrated deformation zones. ASTM A36 displays higher displacements with more uniform and progressive deformation, indicating superior ductility and energy dissipation. Mild Steel's displacement and deformation characteristics fall intermediate between the two, reflecting a balance between strength and flexibility in the structural response. As a preliminary conclusion, ASTM A36 excels in ductility and stable deformation, making it suitable for applications demanding high energy absorption. Mild Steel offers a balanced solution with good strength and flexibility. ASTM 1045 is ideal for structures that require high strength and stiffness, while also offering limited deformation capacity.

3.2. Effect of Core Geometry

Variations in the core geometry of sandwich shell structures significantly influence the distribution of stress, strength, and stiffness of the material. Different shapes and configurations of core reinforcements are designed to optimize the structure's capacity to withstand mechanical loads while minimizing stress concentrations that could lead to failure. Simulations using these diverse geometries produced varying Von Mises stress contours. Illustrations of the Von Mises contours and displacement graphs for each geometry and material variation are shown in Figure 15 to 20.

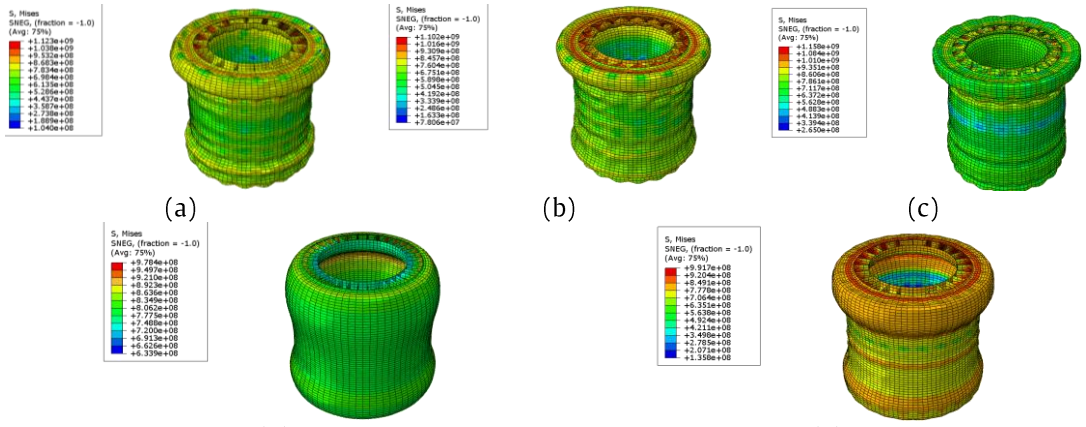

Figure 15. Von-Mises Stress Contour for Mild Steel with Geometry Variations: (a) Geometry 1, (b) Geometry 2, (c) Geometry 3, (d) Geometry 4, and (e) Geometry 5

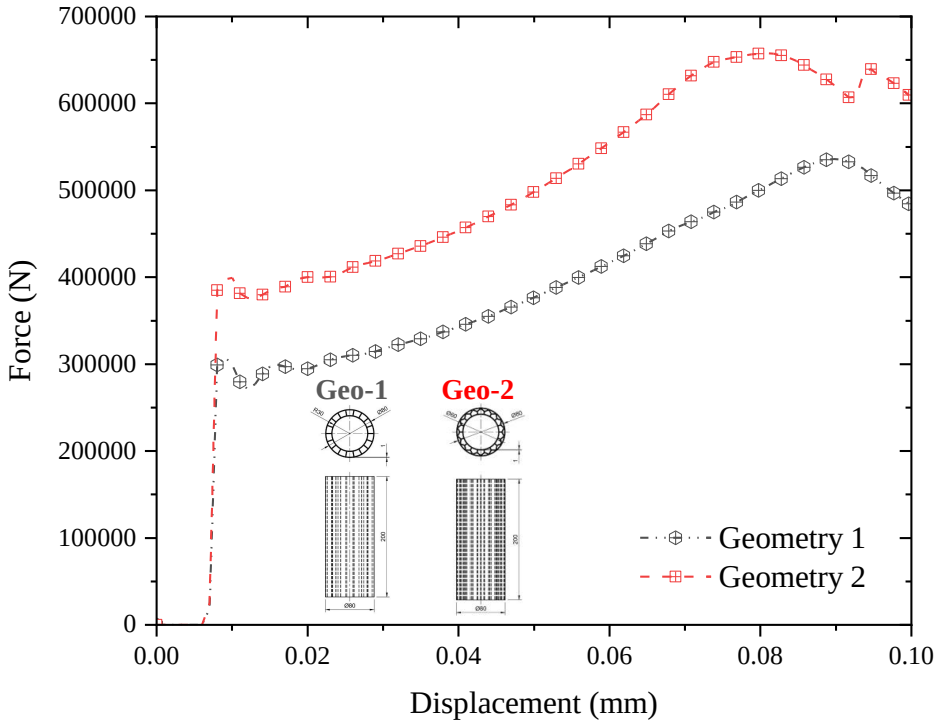

Figure 16. Displacement Graph of Mild Steel: Geometry 1 vs. Geometry 2

The variations in core geometry for mild steel material, as depicted in Figure 15, demonstrate significant differences in stress distribution. Geometry 1, with widely spaced longitudinal reinforcements, exhibits high stress concentration at the junctions between the vertical reinforcement and both the top and bottom plates, indicating uneven load distribution and potential failure risk in these areas. Conversely, Geometry 2, with a diagonal grid pattern that forms a diamond shell, effectively distributes stress evenly across the entire surface, eliminating extreme stress concentrations. Geometry 3 utilizes ring-shaped reinforcements that channel stress through horizontal rings, serving as the primary elements for resisting radial loads. Geometries 4 and 5, featuring varied densities of longitudinal reinforcements, show proportional improvements in stress distribution corresponding to the increased vertical reinforcement density.

From a mechanical performance perspective, as seen in the force-displacement graph in Figure 16, Geometry 2 outperforms Geometry 1. The force-displacement curve for Geometry 2 (marked in red) shows smaller deformation values at equivalent force levels, indicating higher stiffness. For instance, under a load of 400,000 N, Geometry 2 deforms approximately 0.04 mm, while Geometry 1 deforms about 0.06 mm. Furthermore, Geometry 2 can support peak loads up to around 650,000 N, surpassing Geometry 1′s peak capacity of 550,000 N. This confirms that using a mesh/grid reinforcement structure instead of widely spaced vertical reinforcements improves load distribution efficiency in multiple directions, resulting in a stronger and stiffer structure.

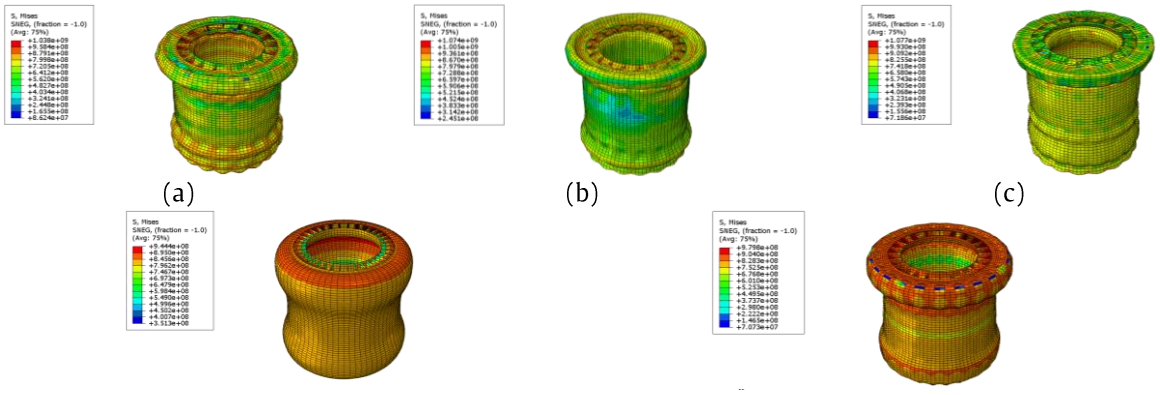

Figure 17. Von-Mises Stress Contour for ASTM A36 with Geometry Variations: (a) Geometry 1, (b) Geometry 2, (c) Geometry 3, (d) Geometry 4, and (e) Geometry 5

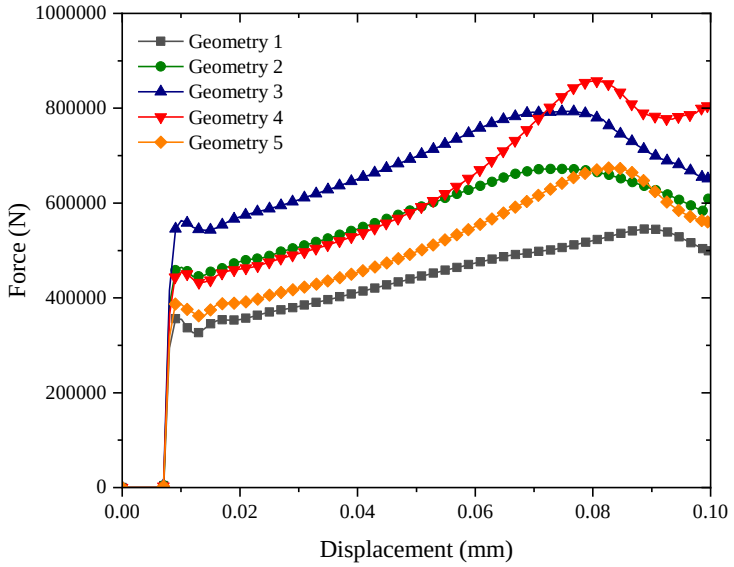

Figure 18. Displacement Graph of ASTM A36 Across Geometry Variations

The Von Mises stress distribution analysis for ASTM A36 material is shown in Figure 17 reveals similar findings. Geometry 1 again exhibits high stress concentrations at the junctions, whereas Geometry 2 distributes stresses more evenly, thereby reducing the areas of extreme stress. Geometry 3 with horizontal ring reinforcements exhibits stress concentrations along the rings. Increasing reinforcement density in Geometries 4 and 5 results in a more uniform stress distribution compared to Geometry 1, although the upper junction area still experiences high stress. Force-displacement curves in Figure 18 rank Geometry 3 highest in strength and lowest in deformation, indicating optimal stiffness, followed by Geometries 2 and 4, with Geometry 1 showing the weakest performance. This highlights the importance of reinforcement design and density in determining structural load-bearing capability.

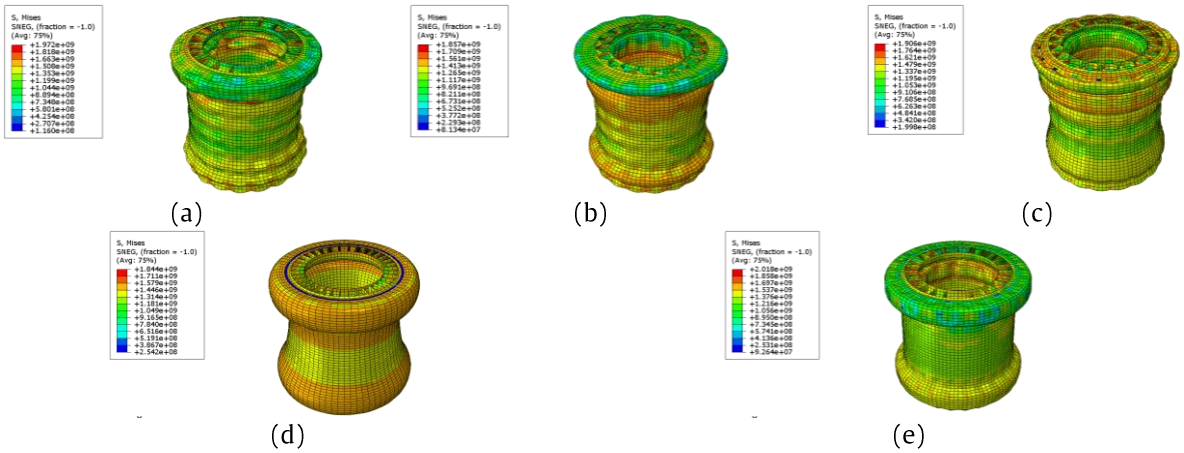

Figure 19. Von-Mises Stress Contour for ASTM 1045 with Geometry Variations: (a) Geometry 1, (b) Geometry 2, (c) Geometry 3, (d) Geometry 4, and (e) Geometry 5

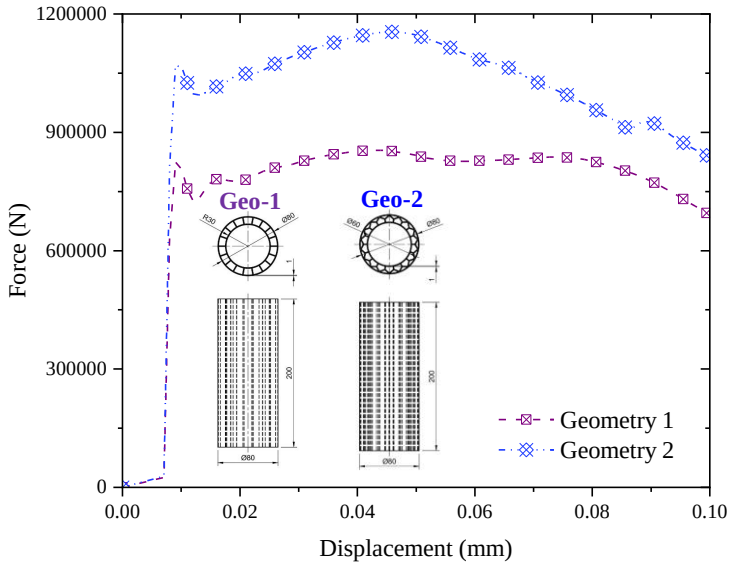

Figure 20. Displacement Graph of ASTM 1045: Geometry 1 vs. Geometry 2

Stress distributions for ASTM 1045 material with all five core geometries accentuate the significant impact of design changes, as illustrated in Figure 19. Geometry 1 with widely spaced longitudinal reinforcements again reveals critical stress concentrations at junctions, while Geometry 2′ s mesh/grid structure evenly distributes stress, mitigating local failure risks. Geometries 3, 4, and 5 show characteristic stress patterns according to their ring shapes and reinforcement densities. Mechanical performance data in Figure 20 reaffirm the superiority of the mesh/grid design (Geometry 2) over Geometry 1, with peak load capacity reaching about 1,100,000 N and improved stiffness, significantly enhancing structural performance.

Therefore, it can be concluded that modifying the core geometry from widely spaced longitudinal reinforcements to mesh/grid structures (Geometry 2) or ring designs (Geometry 3) has a significant influence on the stress distribution and mechanical performance of sandwich shell structures. Mesh/grid-based structures consistently demonstrate more efficient load distribution, higher peak strength, and better stiffness than widely spaced vertical reinforcements. Additionally, ring-shaped reinforcements provide superior resistance to radial loads and optimize stiffness. Therefore, selecting and optimizing core geometry is a key factor in improving durability and structural efficiency under pressure.

3.3. Effect of Energy Absorption

Based on the analysis of the total energy absorption (EA) capacity across various tested materials and geometries, two critical findings emerge in evaluating structural performance against impact. First, ASTM 1045 material consistently exhibits the highest energy absorption values across all geometric variations, indicating that material properties such as yield strength and ductility play a dominant role in determining total EA capacity. Second, among the five geometric designs analysed, Geometry 3 consistently shows the highest energy absorption capacity for each material type. The combination of ASTM 1045 material and Geometry 3 represents the most optimal design choice as it provides maximum energy absorption capacity, which is crucial for minimizing damage caused by dynamic loads.

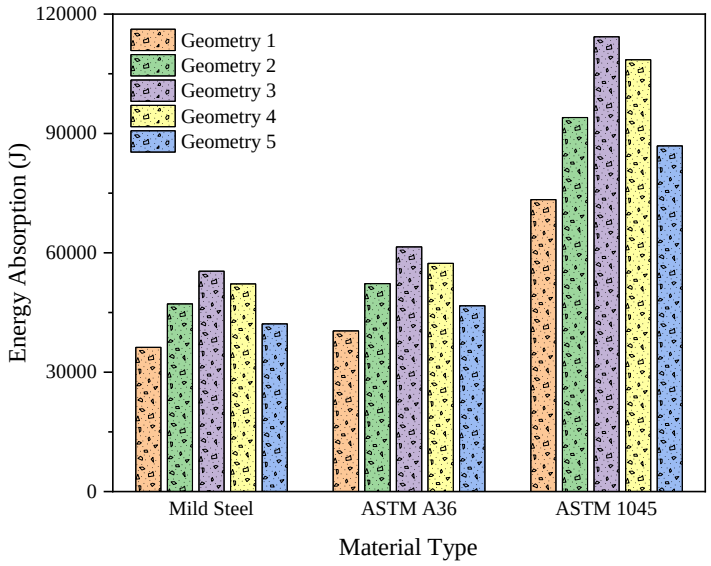

Figure 21. Total Energy Absorption (EA) for Each Variation

Furthermore, this study also evaluates variations in Maximum Compressive Force (MCF) based on numerical simulations of sandwich shells with various materials and geometries. Considering the Coulomb failure theory, the differences in energy absorption among these variations are apparent in Figure 21. Consistent with previous findings, ASTM 1045 shows the highest energy absorption, and Geometry 3 demonstrates the best performance in energy absorption across all material types tested.

4. Conclusion

Based on the tests conducted, several key conclusions can be drawn comprehensively. Material differences significantly impact the von Mises stress values, with ASTM 1045 exhibiting the highest stress levels compared to ASTM A36 and Mild Steel, which have higher elasticity, resulting in lower stress values. Regarding material displacement, ASTM 1045 exhibits the greatest displacement, indicating more significant deformation, even though displacement values for other materials are quite similar. Furthermore, geometry variations affect the distribution of stress and strain contours, with displacement values increasing proportionally to the applied force, followed by a decrease in force once the material reaches its yield strength. Lastly, the optimal combination was found to be Geometry 4 with ASTM 1045, as the most potent combination, requiring the highest force to achieve the desired displacement. In contrast, Geometry 1 with Mild Steel represents the most elastic combination, needing less force to reach the same displacement.

Acknowledgment

This work was supported by the RKAT Universitas Sebelas Maret - Year 2025, under the Research Scheme of "PENGUATAN KAPASITAS GRUP RISET" (PKGR-UNS) A, with research grant/contract no. 371/UN27.22/PT.01.03/2025. The authors highly acknowledge this support.

References

[1] F. T. Hasanah, " Karakteristik wilayah daratan dan perairan di Indonesia," *Jurnal Geografi*, vol. 20, no. 13, pp. 1– 6, 2020 (in Indonesian).

[2] O. O. Husen, N. Abdullah, E. R. Farastuti, A. Rumondang, M. A. Huda, S. Gaffar, K. H. Rombe, D. Rosalina, D. Lesmana, Y. Wahyudin, T. Nisari, R. M. Rachman, N. Kartini, and H. Irawan, Potensi dan Pengelolaan Sumber Daya Kelautan Indonesia, PT. Kamiya Jaya Aquatic, Ternate, Indonesia, 2024.

[3] M. Safarabadi, M. Haghighi-Yazdi, M. Sorkhi, and A. Yousefi, " Experimental and numerical study of buckling behavior of foam-filled honeycomb core sandwich panels considering viscoelastic effects," *Journal of Sandwich Structures & Materials*, vol. 23, no. 11, pp. 3985– 4015, 2021, doi: https://doi.org/10.1177/1099636220975168.

[4] L. Tripathi and B. Behera, " Comparative analysis of aluminium core honeycomb with 3D woven Kevlar honeycomb composite," *Material Science and Technology*, vol. 39, no. 10, pp. 1697– 1708, 2023, doi: https://doi.org/10.1080/02670836.2023.2180601.

[5] A. Yadav, M. Amabili, S. K. Panda, and T. Dey, "Nonlinear analysis of cylindrical sandwich shells with porous core and CNT reinforced face-sheets by higher-order thickness and shear deformation theory," *European Journal of Mechanics - A/Solids*, vol. 90, article no. 104366, 2021 doi: https://doi.org/10.1016/j.euromechsol.2021.104366

[6] H. Manjunatha, K. V. Ratnam, S. Janardan, R. V. Nadh, N. S. Kumar, N. V. K. Prasad, S. Ramesh, K. C. B. Naidu, and T. A. Babu, " Marine Corrosion," in Corrosion Science: Modern Trends and Applications, Bentham Science, Sharjah, United Arab Emirates, 2020, doi: https://doi.org/10.2174/9789811481833121010014.

[7] M. Chairi et al., " The effect of span length on the flexural properties of glass and basalt fiber reinforced sandwich structures with balsa wood core for sustainable shipbuilding," *Composite Structure*, vol. 343, p. 118187, 2024, doi: https://doi.org/10.1016/j.compstruct.2024.118187.

[8] G. Di Bella and G. Palomba, " Cork/aluminium double-layer sandwich panels under impact loading for lightweight ship structures," *International Journal of Crashworthiness*, vol. 28, no. 8, pp. 797– 808, 2023, doi: https://doi.org/10.1080/13588265.2022.2130619.

[9] J. Blanchard and A. Sobey, " Sustainable Sandwich Panels for Use in Ship Superstructures," in Lecture Notes in Civil Engineering, Singapore: Springer, 2019, pp. 135– 144. doi: https://doi.org/10.1007/978-981-15-4672-3_14.

[10] Y. Garbatov, G. Palomba, and V. Crupi, " Risk-Based Hybrid Light-Weight Ship Structural Design Accounting for Carbon Footprint," *Applied Science*, vol. 13, no. 6, article no. 3583, 2023, doi: https://doi.org/10.3390/app13063583.

[11] EMSA, "Annual Overview of Marine Casualties and Incidents 2017," European Maritime Safety Agency, Lisbon, Portugal, 2017.

[12] A. D. Saputra, "Studi kecelakaan kapal di Indonesia dari tahun 2003-2019 berdasarkan data investigasi Komite Nasional Keselamatan Transportasi," *Warta Penelitian Perhubungan*, vol. 33, no. 2, pp. 87-94, 2021 doi: https://doi.org/10.25104/warlit.v33i2.1502

[13] A. A. Pratama et al., " Hollow tube structures subjected to compressive loading: implementation of the pitting corrosion effect in nonlinear FE analysis," *Journal of the Brazilian Society of Mechanical Sciences and Engineering*, vol. 45, no. 3, article no. 154, 2023, doi: https://doi.org/10.1007/s40430-023-04067-3.

[14] G. J. Shi, D. Y. Wang, B. Hu, and S. J. Cai, " Effect of initial geometric imperfections on dynamic ultimate strength of stiffened plate under axial compression for ship structures," *Ocean Engineering*, vol. 256, article no. 111448, 2022, doi: https://doi.org/10.1016/j.oceaneng.2022.111448.

[15] S. K. Tak and M. A. Iqbal, " Axial compression behaviour of thin-walled metallic tubes under quasi-static and dynamic loading," *Thin-Walled Structure*, vol. 159, article no. 107261, 2021, doi: https://doi.org/10.1016/J.TWS.2020.107261.

[16] R. Yao, T. Pang, B. Zhang, J. Fang, Q. Li, and G. Sun, " On the crashworthiness of thin-walled multi-cell structures and materials: State of the art and prospects," *Thin-Walled Structure*, vol. 186, article no. 110734, 2023, doi: https://doi.org/10.1016/j.tws.2023.110734.

[17] G. R. Johnson and W. H. Cook, " Fracture characteristics of three metals subjected to various strains, strain rates, temperatures and pressures," *Engineering Fracture Mechanics*, vol. 21, no. 1, pp. 31– 48, 1985, doi: https://doi.org/10.1016/0013-7944(85)90052-9.

[18] H. A. Al Kautsar et al., " Structural Analysis of Designed Tubes Under Axial Compression: Variations of Applied Temperature, Material Type, and Geometry Design," *Communications - Scientific Letters of the University of Zilina*, vol. 26, no. 3, pp. B199– B215, 2024, doi: https://doi.org/10.26552/com.C.2024.036

[19] M. F. Dzulfiqar, A. R. Prabowo, R. Ridwan, and H. Nubli, " Assessment on the designed structural frame of the automatic thickness checking machine - Numerical validation in FE method," *Procedia Structural Integrity*, vol. 35, pp. 59– 66, 2021, doi: https://doi.org/10.1016/j.prostr.2021.10.009.

[20] M. Dundar, K. Ercan, and O. Özenç, " Comparative assessment of element types for evaluating local elastic buckling behavior of rectangular hollow sections using finite element analysis," *Journal of Innovative Engineering and Natural Science*, vol. 4, no. 2, pp. 127-146, 2024, doi: https://doi.org/10.61112/jiens.1555378.